nature microbiology

ARTICLES

https://doi.org/10.1038/s41564-018-0341-1

Divergent rRNAs as regulators of gene expression at the ribosome level

Wooseok Song[1,8], Minju Joo[1,8], Ji-Hyun Yeom[1,8], Eunkyoung Shin[2,8], Minho Lee[1,8], Hyung-Kyoon Choi[2], Jihwan Hwang[3], Yong-In Kim[4], Ramin Seo[4,5], J. Eugene Lee[4], Christopher J. Moore[6], Yong-Hak Kim[7], Seong-il Eyun[1], Yoonsoo Hahn[1], Jeehyeon Bae[2*] and Kangseok Lee[1*]

It is generally assumed that each organism has evolved to possess a unique ribosomal RNA (rRNA) species optimal for its physiological needs. However, some organisms express divergent rRNAs, the functional roles of which remain unknown. Here, we show that ribosomes containing the most variable rRNAs, encoded by the *rrnI* operon (herein designated as I-ribosomes), direct the preferential translation of a subset of mRNAs in *Vibrio vulnificus*, enabling the rapid adaptation of bacteria to temperature and nutrient shifts. In addition, genetic and functional analyses of I-ribosomes and target mRNAs suggest that both I-ribosomal subunits are required for the preferential translation of specific mRNAs, the Shine–Dalgarno sequences of which do not play a critical role in I-ribosome binding. This study identifies genome-encoded divergent rRNAs as regulators of gene expression at the ribosome level, providing an additional level of regulation of gene expression in bacteria in response to environmental changes.

Ribosomes constitute the protein synthesis machinery and are composed of rRNAs and polypeptides. It has been demonstrated that rRNA has a major role in ribosome function[1]. In most organisms, rRNA genes are present in multiple copies that produce nearly identical mature rRNAs[2,3]. It is assumed that organisms have evolved to possess unique rRNA species optimal for their physiological needs via homogenization of the rRNA gene copies through gene conversion[4]. However, significant degrees of dissimilarity in the rRNA sequences of individual organisms have been discovered in all three domains of life[5–13]. For instance, bacterial species with sequences that differ by more than 1% are common[14]. This variability in the rRNA sequences of individual organisms poses a problem in estimating the evolutionary history and in making taxonomic assignments of these organisms[14,15].

While the existence of species-specific genome-encoded divergent rRNAs has been acknowledged for decades, their physiological roles remain largely unknown. In the case of the malaria-causing *Plasmodium* parasites, two different types of rRNAs are expressed at different developmental stages[7,16]. However, the two types of rRNAs have been suggested to be functionally equivalent[17,18]. In halophilic archaea *Haloarcula* species, genome-encoded divergent rRNAs are differentially expressed and are required for rapid growth at high temperatures[19,20]. In *Escherichia coli*, subpopulations of heterogeneous ribosomes containing rRNAs with sequence-specific differences were proposed to have the ability to regulate the expression of stress response genes via an unknown mechanism[21].

There are also examples of variant rRNAs that are produced by endoribonucleases in *E. coli*. MazF generates 16S rRNAs without the anti-Shine–Dalgarno (ASD) sequence that usually interacts with the Shine–Dalgarno (SD) sequence in the 5′ untranslated region (UTR) of mRNAs[22,23]. However, the existence of specialized ribosomes containing MazF-processed 16S rRNA and their functional role are still under debate[24–26]. Another *E. coli* endoribonuclease, RNase G, also participates in the generation of heterogeneous 16S rRNAs when *E. coli* cells are exposed to aminoglycoside antibiotics[27,28]. Under these conditions, the accumulation of incompletely processed 16S rRNA precursors via the downregulation of RNase G expression results in the generation of a subpopulation of heterogeneous ribosomes. These render *E. coli* cells resistant to aminoglycoside antibiotics.

Emerging evidence suggests that the ribosome has an intrinsic regulatory capacity in mRNA translation mediated by the heterogeneity of the ribosome composition (for recent reviews, see refs. [29–31]). In this study, we investigated a possible physiological role of genome-encoded divergent rRNAs and their mechanism of action in the marine pathogenic bacterium *V. vulnificus* CMCP6.

Results

Identification of mRNAs with *rrnI*-dependent expression. Among the divergent rRNAs of *V. vulnificus* CMCP6, rRNAs encoded by the *rrnI* operon (I-rRNA), which is present solely on chromosome II, are the most divergent[8] (Supplementary Table 1). For this reason, in this study, divergent I-rRNAs were chosen for functional analyses.

First, *rrnI*-deleted (Δ*rrnI* + pRK415; Δ*rrnI*) and *rrnI*-complemented (Δ*rrnI* + pRK415-*rrnI*; Δ*rrnI*^{comp}) strains were constructed and characterized. In addition, a *rrnG*-deleted (Δ*rrnG*) strain was used to control for the effect of rRNA gene copy number variation, since the *rrnG* operon encodes the most redundant rRNAs in *V. vulnificus*. Depletion and overexpression of I-rRNAs and the

[1]Department of Life Science, Chung-Ang University, Seoul, Republic of Korea. [2]School of Pharmacy, Chung-Ang University, Seoul, Republic of Korea. [3]Department of Microbiology, Pusan National University, Busan, Republic of Korea. [4]Center for Bioanalysis, Korea Research Institute of Standards and Science, Daejeon, Republic of Korea. [5]Department of Biological Sciences, Korea Advanced Institute of Science and Technology, Daejeon, Republic of Korea. [6]Department of Genetics, Stanford University, Stanford, CA, USA. [7]Department of Microbiology, Catholic University of Daegu School of Medicine, Daegu, Republic of Korea. [8]These authors contributed equally: Wooseok Song, Minju Joo, Ji-Hyun Yeom, Eunkyoung Shin and Minho Lee. *e-mail: jeehyeon@cau.ac.kr; kangseok@cau.ac.kr

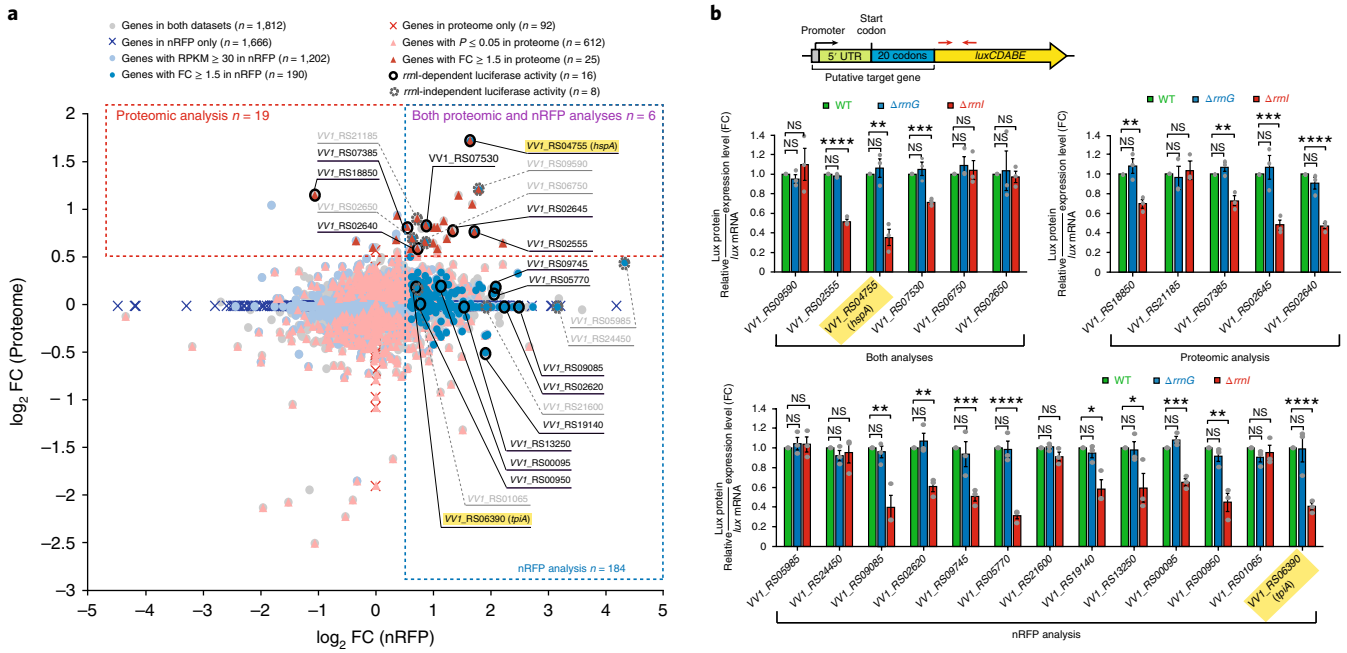

Fig. 1 | Identification of mRNAs with *rrnI*-dependent expression. a, Distribution of genes identified from comparative analyses of ribosome profiling and proteome data in the Δ*rrnI* and Δ*rrnI*^{comp} strains. Pale blue and pale red filled circles indicate 1,202 genes from ribosome profiling analysis (Supplementary Table 2) and 612 genes from proteomic analysis (Supplementary Table 4), respectively, selected by the filtering criteria described in the Methods. Among these genes, 190 from the ribosome profiling analysis (Supplementary Table 3) and 25 from the proteomic analysis that exhibited significant increases of more than 1.5-fold change (FC) in Δ*rrnI*^{comp} cells compared with Δ*rrnI* cells are highlighted in dark blue and dark red, respectively. Data points with no values or statistically non-significant values are indicated by Xs. Genes showing *rrnI*-expression-dependent and -independent luciferase report activity (Fig. 1b) are indicated by black and grey filled circles, respectively. The nRFP was calculated by dividing the ribosome footprint (RFP), as determined by ribosome profiling, by the mRNA abundance, as determined by total RNA-sequencing. **b**, Characterization of *rrnI*-dependent expression of putative target mRNAs identified by ribosome profiling and proteomic analyses. Top: for each gene, a DNA fragment containing the putative intact promoter, the 5′ UTR and the CDS for the first 20 amino acids was cloned in-frame with the CDS of the luciferase gene in the pBBR-lux vector[61], which contains a promoterless *luxCDABE* reporter. Bottom: WT, Δ*rrnG* and Δ*rrnI* strains harbouring luciferase reporter constructs were grown in LBS medium at 30 °C until the OD_{600} reached 1.0, and the relative expression level of *lux* was measured. Luciferase activities were normalized using *lux* reporter mRNA levels (Supplementary Fig. 3b). The expression levels of *lux* were compared by setting those of the WT to 1. The data are presented as the mean ± s.e.m. of three independent experiments. *$P < 0.05$, **$P < 0.01$, ***$P < 0.001$, ****$P < 0.0001$ denote significant differences as determined via two-sided unpaired Student's *t*-tests. NS, not significant. Red arrows indicate the primers used in qPCR. The genes (*hspA* and *tpiA*) that were further analysed for *rrnI*-dependent expression are highlighted.

incorporation of exogenously expressed I-rRNAs into ribosomes were assessed by allele-specific quantitative PCR (qPCR) (Supplementary Fig. 1a). The rRNAs from the *rrnI* operon represented ~10% of the total rRNAs in the wild-type (WT) and Δ*rrnG* strains, whereas they corresponded to ~30% of the total rRNAs in the Δ*rrnI*^{comp} strain. Analogous results were obtained when the distribution and incorporation of the 23S I-rRNA in 70S ribosomes were characterized in these strains using a modified primer extension method (Supplementary Fig. 1b).

Next, we sought to identify genes for which expression was potentially regulated in an I-rRNA expression-dependent manner. To this end, the normalized ribosome footprint (nRFP) of each mRNA and relative abundance of total cellular proteins were analysed in the Δ*rrnI* and Δ*rrnI*^{comp} strains. The nRFP was assesed by deep sequencing, whereas the cellular protein abundance was assessed by mass spectrometry (MS) using tandem mass tag (TMT) technology (Supplementary Tables 2, 3 and 4). For these experiments, we performed comparative analyses of ribosome profiling and proteome data between the Δ*rrnI* and Δ*rrnI*^{comp} strains. We reasoned that comparative analyses of datasets between the *rrnI*-overexpressing and *rrnI*-deleted strains would reduce the possibility of excluding true positive genes for which expression is regulated in an I-rRNA expression-dependent manner.

By integrating the nRFP and relative protein abundance lists, only six genes were identified for which the nRFP and protein abundance were simultaneously increased by more than 1.5-fold in Δ*rrnI*^{comp} cells compared with that in Δ*rrnI* cells. The remaining genes (184 genes from the nRFP analysis and 19 genes from the proteomic analysis) were either not detected or not significantly increased in one of the two analyses (Fig. 1a; Supplementary Fig. 2).

Since ribosome profiling and proteomic analyses are simply tools for discovering genes with expression patterns associated with I-rRNA expression levels, 24 genes with higher fold changes or whose products showed annotations of interest were selected for further analysis using luciferase reporter constructs (Fig. 1b; Supplementary Discussion). Reduced luciferase reporter activity was observed specifically in the Δ*rrnI* strain for 16 out of the 24 tested genes. Nine out of 13 positive genes and 4 out of 5 positive genes from the ribosome profiling and proteome data, respectively, which were identified as positives in only one of the two datasets, showed *rrnI* expression-dependent reporter activity (Fig. 1b; Supplementary Fig. 3a). For those identified as positives in both datasets, three out of six positive clones showed decreased activity specifically in the Δ*rrnI* strain (Fig. 1b; Supplementary Fig. 3a). The expression levels of the luciferase (*lux*) reporter mRNA

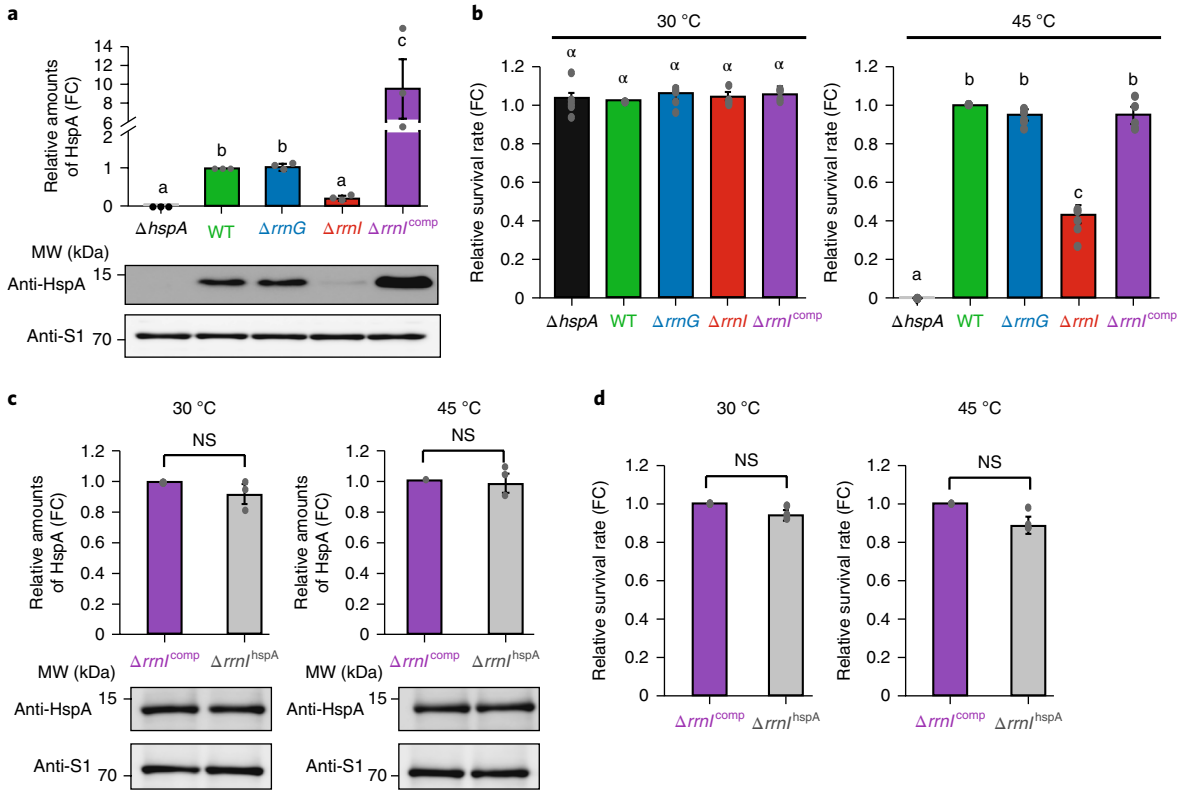

Fig. 2 | *rrnI*-dependent expression of *hspA*. a, *rrnI*-dependent expression of HspA. *V. vulnificus* strains (WT, Δ*rrnG*, Δ*rrnI*, Δ*rrnI*^{comp} and Δ*hspA*) were grown in LBS at 30 °C to mid-log phase and were collected for western blot analysis of HspA using polyclonal antibodies against HspA. **b**, Effect of *rrnI* expression on heat shock susceptibility of *V. vulnificus*. CFUs of the *V. vulnificus* cultures used in **a**, as well as of cultures transiently grown at 45 °C for 180 min, were measured. The expression levels of HspA and the number of CFUs were compared by setting those of the WT to 1. The data are presented as the mean ± s.e.m. of three independent experiments, and significant differences are indicated with different letters (one-way analysis of variance (ANOVA) with Student–Newman–Keuls test, $P < 0.0001$; Greek symbols indicate the difference from 30 °C; English letters indicate the difference from 45 °C). **c**, Expression levels of HspA in Δ*rrnI*^{comp} and Δ*rrnI*^{hspA} (Δ*rrnI* + pRK415-*hspA*). Δ*rrnI*^{comp} and Δ*rrnI*^{hspA} were grown in LBS at 30 °C to mid-log phase or were further incubated at 45 °C for 180 min and collected for western blot analysis of HspA using polyclonal antibodies against HspA. **d**, Effect of exogenous expression of *hspA* on heat shock susceptibility of Δ*rrnI* cells. Δ*rrnI*^{comp} and Δ*rrnI*^{hspA} cells were grown in LBS medium at 30 °C to mid-log phase or were further incubated at 45 °C for 180 min. Then, the cultures were diluted and plated on LBS agar plates for measurement of CFUs. The expression levels of HspA and the number of CFUs were compared by setting those of Δ*rrnI*^{comp} to 1. The data are presented as the mean ± s.e.m. of three independent experiments. Two-sided unpaired Student's *t*-test. For **a** and **c**, the S1 protein was used as an internal standard to evaluate the amount of cell extract in each lane.

were not significantly altered in any of the strains used in these experiments (Supplementary Fig. 3b,c). These results suggest that a subgroup of mRNA species is preferentially translated by ribosomes containing I-rRNAs.

Effect of *rrnI* expression on *hspA* expression and heat shock susceptibility of *V. vulnificus*. Next, we investigated whether the expression levels of the protein products from the previously identified genes were reduced in Δ*rrnI* cells, and, if so, whether this downregulation led to phenotypic changes. To this end, we analysed the effect of *rrnI* deletion on the expression of the protein encoded by the *VV1_RS04755* gene. The protein product of this gene was the most overexpressed in the Δ*rrnI*^{comp} strain compared with the relative abundance of total cellular proteins in the Δ*rrnI* and Δ*rrnI*^{comp} strains (Supplementary Table 4). *VV1_RS04755* encodes a putative heat shock protein (herein designated as HspA) that shows high sequence homology (80% amino acid similarity) to the *E. coli* heat shock protein IbpA[32]. Expression of HspA decreased by ~80% in the Δ*rrnI* strain and increased by nearly 9.5-fold in the Δ*rrnI*^{comp} strain compared with levels in WT cells. Conversely, deletion of *rrnG* did not significantly affect the expression of HspA (Fig. 2a). The mRNA expression of *hspA* was not significantly changed in any strain except the Δ*hspA* strain (Supplementary Fig. 4a). The *rrnI* expression-dependent changes in HspA expression were strongly associated with heat shock susceptibility in *V. vulnificus*. Specifically, heat shock at 45 °C for 180 min resulted in an ~60% decrease in colony forming units (CFUs) in the Δ*rrnI* strain compared with that in the WT strain. By contrast, no significant changes in CFU numbers were detected in the Δ*rrnG* strain compared with that in the WT strain (Fig. 2b). The increased heat shock susceptibility of the Δ*rrnI* cells was restored to WT levels when *rrnI* was exogenously expressed in these cells (Δ*rrnI*^{comp}) (Fig. 2b). Furthermore, deletion of the *hspA* gene completely abolished the ability of *V. vulnificus* cells to produce CFUs after heat shock (Fig. 2b). In addition, heat shock susceptibility in Δ*rrnI* cells was restored to WT levels when the *hspA* gene was exogenously expressed (Δ*rrnI*^{hspA}) (Fig. 2c,d). Conversely, no significant change in heat shock susceptibility of WT cells was observed when the *hspA* gene was exogenously expressed (WT^{hspA}) (Supplementary Fig. 5). Thus, these results show that the increased heat shock susceptibility of Δ*rrnI* cells is a direct consequence of the downregulation of *hspA* expression in these cells.

Effect of *rrnI* expression on *tpiA* expression and the ability of *V. vulnificus* to utilize glycerol as the sole carbon source. We next investigated the effect of *rrnI* expression on *V. vulnificus* carbon metabolism. This was pursued because numerous genes whose nRFP was strongly increased in *rrnI*-overexpressing cells appeared to encode proteins involved in carbon metabolism (Supplementary Table 3). Among these genes, expression of the protein encoded by the *VV1_RS06390* gene, a putative triosephosphate isomerase (herein designated as TpiA), and its effect on *V. vulnificus* carbon metabolism were analysed. TpiA was chosen because its enzymatic activity provides an easy method of detecting phenotypic changes in carbon metabolism. In *E. coli* grown with glycerol as the sole carbon source, downregulation of *tpiA* results in growth defects due to the accumulation of methylglyoxal[33,34]. TpiA expression decreased by ~47% in Δ*rrnI* cells and increased by ~58% in Δ*rrnI*^{comp} cells compared with levels in WT cells (Fig. 3a). Deletion of *rrnG* did not significantly affect the expression of TpiA (Fig. 3a). The mRNA expression of *tpiA* was not significantly changed in any strain except the Δ*tpiA* strain (Supplementary Fig. 4b). Minimal growth was observed when Δ*rrnI* cells were cultured in minimal medium with 40 mM glycerol, whereas WT, Δ*rrnG* and Δ*rrnI*^{comp} cells grew normally, with comparable growth rates under the same conditions (Fig. 3b). When minimal medium with 20 mM glucose was used, all the strains grew well with no significant changes in their growth rates. However, the growth yield of the Δ*rrnI* and Δ*rrnI*^{comp} strains was lower than that of the other strains (Fig. 3b). In agreement with the observed growth rate in glycerol medium and TpiA expression in these strains, the extracellular concentration of methylglyoxal was approximately two times higher in Δ*rrnI* cells compared with that in WT cells. The level of methylglyoxal in the Δ*rrnI*^{comp} strain was restored to WT levels (Fig. 3c). However, the growth defect of Δ*rrnI* cells in glycerol medium was not fully restored when *tpiA* was exogenously expressed in these cells (Δ*rrnI*^{tpiA}). This indicates that additional downregulated genes involved in carbon metabolism are also involved in the decreased ability of Δ*rrnI* cells to utilize glycerol as the sole carbon source (Fig. 3d,e).

Effect of *rrnI* deletion on *V. vulnificus* virulence in mice. *V. vulnificus* is a highly virulent, opportunistic pathogen that causes gastroenteritis, primary sepsis and wound infection in humans[35]. *V. vulnificus* spreads rapidly and causes extensive tissue damage, leading to a mortality rate of over 50% among infected patients with sepsis[36]. For this reason, we investigated whether the absence of *rrnI* expression affects the ability of *V. vulnificus* to adapt to its host environment. For this purpose, the WT, Δ*rrnI* and Δ*rrnG* strains were injected intraperitoneally into mice, and the duration and rates of survival of the infected mice were assessed. Higher survival rates were observed in Δ*rrnI*-infected mice compared with that in mice infected with the WT or Δ*rrnG* strains (Fig. 4a). The rRNAs from the *rrnI* operon represented ~10% of the total rRNAs in the spleen, liver and mesenteric lymph nodes of mice that were infected with WT *V. vulnificus* cells. This indicated that I-rRNA expression levels do not significantly change in relation to other rRNAs during infection in mice (Fig. 4b). Furthermore, we investigated virulence factors for which expression is regulated by *rrnI* expression. We measured the survival rates and duration of survival of mice infected with WT or *hspA*- or *tpiA*-deleted strains. The results indicated that *tpiA* is a virulence factor as we observed decreased survival of the Δ*rrnI* strain in mice (Fig. 4c).

Identification of variable I-rRNA residues associated with *rrnI*-dependent translation of *hspA* mRNAs. In the canonical mechanism of bacterial translation, mRNAs are selected by the 30S subunit. This selection is accomplished by the interaction between the SD sequence in the 5′ UTR of the mRNA and the ASD sequence in the 3′ end of the 16S rRNA[23]. Therefore, we reasoned that the 16S I-rRNA is likely to be responsible for the *rrnI*-dependent translation of *hspA* mRNAs. However, expression of the 16S I-rRNA only in Δ*rrnI* cells resulted in HspA expression levels similar to those found in Δ*rrnI* cells harbouring an empty vector (Fig. 5a; Supplementary Fig. 4c). Consequently, heat shock resistance was not restored to WT levels (Fig. 5b). The separate expression of the 23S or the 5S I-rRNAs of the *rrnI* operon also failed to restore HspA expression or heat shock resistance in the Δ*rrnI* strain (Fig. 5a,b; Supplementary Fig. 4c). The proportion of I-rRNAs expressed from these chimeric rRNA genes in ribosomes was comparable to that in Δ*rrnI*^{comp} cells (Fig. 5c). These results indicate that ribosomes containing both the 16S and 23S I-rRNAs (I-ribosomes) are required for enhanced translation of *hspA* mRNA.

We further investigated whether I-ribosome-mediated phenotypic changes are associated with the perturbation of ribosome biogenesis by measuring the number of ribosomes per cell in WT, Δ*rrnG*, Δ*rrnI*, Δ*rrnI*^{comp}, Δ*rrnI*+I^{16S}/G^{23S+5S} and Δ*rrnI*+G^{16S}/I^{23S+5S} strains. We observed that strains with the deletion of a single *rrn* operon (Δ*rrnG* and Δ*rrnI*) showed an ~10% reduction in the number of ribosomes per cell. Conversely, strains overexpressing rRNAs from a cloned, plasmid-borne copy of the *rrn* operon (Δ*rrnI*^{comp}, Δ*rrnI*+I^{16S}/G^{23S+5S} and Δ*rrnI*+G^{16S}/I^{23S+5S}) showed an ~10% increase in the number of ribosomes per cell compared with that in the WT strain (Fig. 5d). These changes in the number of ribosomes per cell in mutated strains did not significantly affect their growth rates in Luria–Bertani with NaCl (LBS) medium. However, the growth yield of the rRNA-overexpressing strains (Δ*rrnI*^{comp}, Δ*rrnI*+I^{16S}/G^{23S+5S} and Δ*rrnI*+G^{16S}/I^{23S+5S}) was lower than that of the other strains (Fig. 5e). These results indicate that I-ribosome-mediated phenotypic changes are unlikely to be associated with the perturbation of ribosome biogenesis.

Next, we investigated which variable residues of the I-rRNAs are responsible for the *rrnI*-mediated enhanced translation of *hspA* mRNA. To this end, variable segments in the I-rRNAs were replaced with those in redundant rRNAs from the *rrnG* operon, and *hspA* translation efficiency was measured. The substitution of residues 101, 302 or a combination of 302 and 342 in the 16S I-rRNA, and substitution of residues 1722 or a combination of 1735, 1736 and 1737 in the 23S I-rRNA resulted in decreased expression levels of HspA compared with levels in Δ*rrnI*^{comp} cells (Fig. 5f). Expression levels of *hspA* mRNA and mutant I-rRNAs were not significantly changed compared with those in the Δ*rrnI*^{comp} strain (Supplementary Fig. 6). These results indicate that a subgroup of variable I-rRNA residues located in regions in close proximity to the intersubunit region (Fig. 5g) contribute to the formation of unique structural determinants required for the I-ribosome-mediated preferential translation of specific mRNAs.

Identification of structural elements in I-ribosome target mRNAs. To understand the molecular mechanisms behind I-ribosome function, we investigated the structural elements in mRNAs that are specifically recognized by I-ribosomes. First, the secondary structure of the region that encompasses the 5′ UTR and the coding sequence (CDS) of the first 20 amino acids was analysed in 15 putative mRNAs, identified in Fig. 1b, using the M-fold program (http://unafold.rna.albany.edu) (Supplementary Fig. 7). The secondary structure of the ribosome binding sites showed that all putative SD sequences were buried in stem–loop or hairpin structures except for one gene (*VV1_RS02620*), which appears to express a leaderless mRNA (Supplementary Fig. 7). We tested whether these structural features affected I-ribosome-mediated discriminative mRNA selection by constructing a *hspA*-RBS::*luc* (SD-MT1) fusion containing the SD sequence that is more accessible to the 30S subunit. We then measured the luciferase activity in WT, Δ*rrnG* and Δ*rrnI* cells. No repression of reporter activity was observed in the Δ*rrnI* strain when the mutant SD was used (Fig. 6a; Supplementary

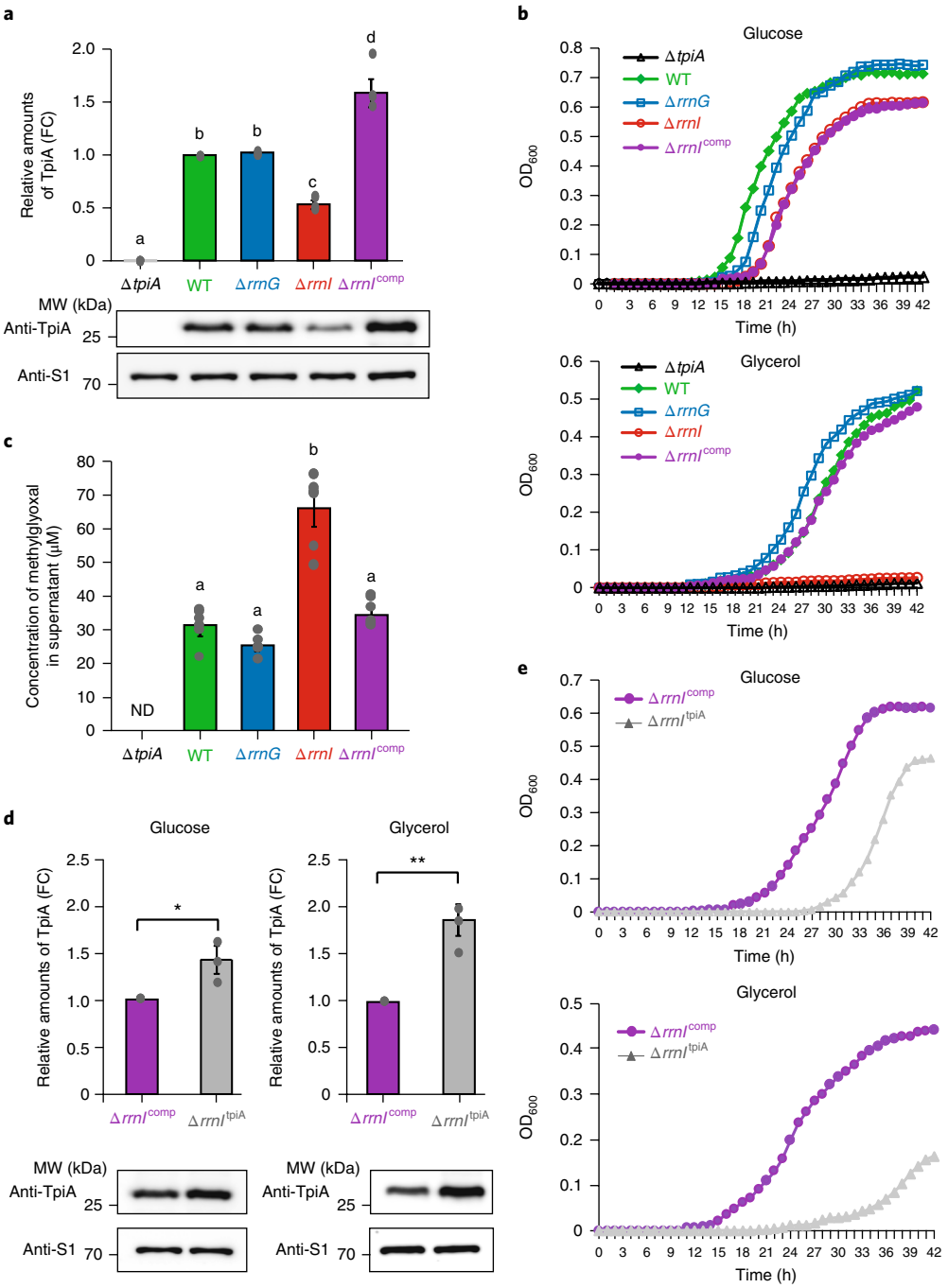

Fig. 3 | *rrnl*-dependent expression of *tpiA* and phenotypic changes in *V. vulnificus*. **a**, *rrnl*-dependent expression of TpiA. *V. vulnificus* strains (WT, Δ*rrnG*, Δ*rrnl*, Δ*rrnl*^{comp} and Δ*tpiA*) grown in glycerol medium at 37 °C were collected for western blot analysis of TpiA using polyclonal antibodies against TpiA. The expression levels of TpiA were compared by setting those of the WT strain to 1. The data are presented as the mean ± s.e.m. of four independent experiments, and significant differences are indicated with different letters (one-way ANOVA with Student–Newman–Keuls test, $P < 0.0001$). **b**, Effect of *rrnl* expression on the ability of *V. vulnificus* to use glycerol as the sole carbon source. The strains used in **a** were grown in minimal medium containing 20 mM glucose or 40 mM glycerol as the carbon source, and their growth was monitored by measuring the OD_{600} at the indicated time points. **c**, Effect of *rrnl* expression on the accumulation of methylglyoxal. The amount of extracellular methylglyoxal was measured in the supernatant of the cultures used in **b** grown in glycerol medium, as described in the Methods. Methylglyoxal interferes with the reversible interconversion of dihydroxyacetone phosphate and D-glyceraldehyde 3-phosphate, an important step in glycolysis[33,34]. The data are presented as the mean ± s.e.m. of six independent experiments, and significant differences are indicated with different letters (one-way ANOVA with Student–Newman–Keuls test, $P < 0.0001$). ND, not determined. **d**, Expression levels of TpiA in Δ*rrnl*^{comp} and Δ*rrnl*^{tpiA} (Δ*rrnl* + pRK415-*tpiA*) strains. Mid-log phase cultures of Δ*rrnl*^{comp} and Δ*rrnl*^{tpiA} cells grown in minimal medium were collected for western blot analysis of TpiA. The expression levels of TpiA were compared by setting those of Δ*rrnl*^{comp} to 1. The data are presented as the mean ± s.e.m. of three independent experiments. $^{*}P < 0.05$, $^{**}P < 0.01$. **e**, Effect of *tpiA* exogenous expression on the growth of Δ*rrnl* cells in minimal medium. Δ*rrnl*^{comp} and Δ*rrnl*^{tpiA} strains were grown at 37 °C in minimal medium containing 20 mM glucose or 40 mM glycerol as the carbon source. Growth of these cultures was monitored by measuring the OD_{600} at the indicated time points. For **a** and **d**, the S1 protein was used as an internal standard to evaluate the amount of cell extract in each lane. For **b** and **e**, data are representative of three independent experiments, and similar results were obtained.

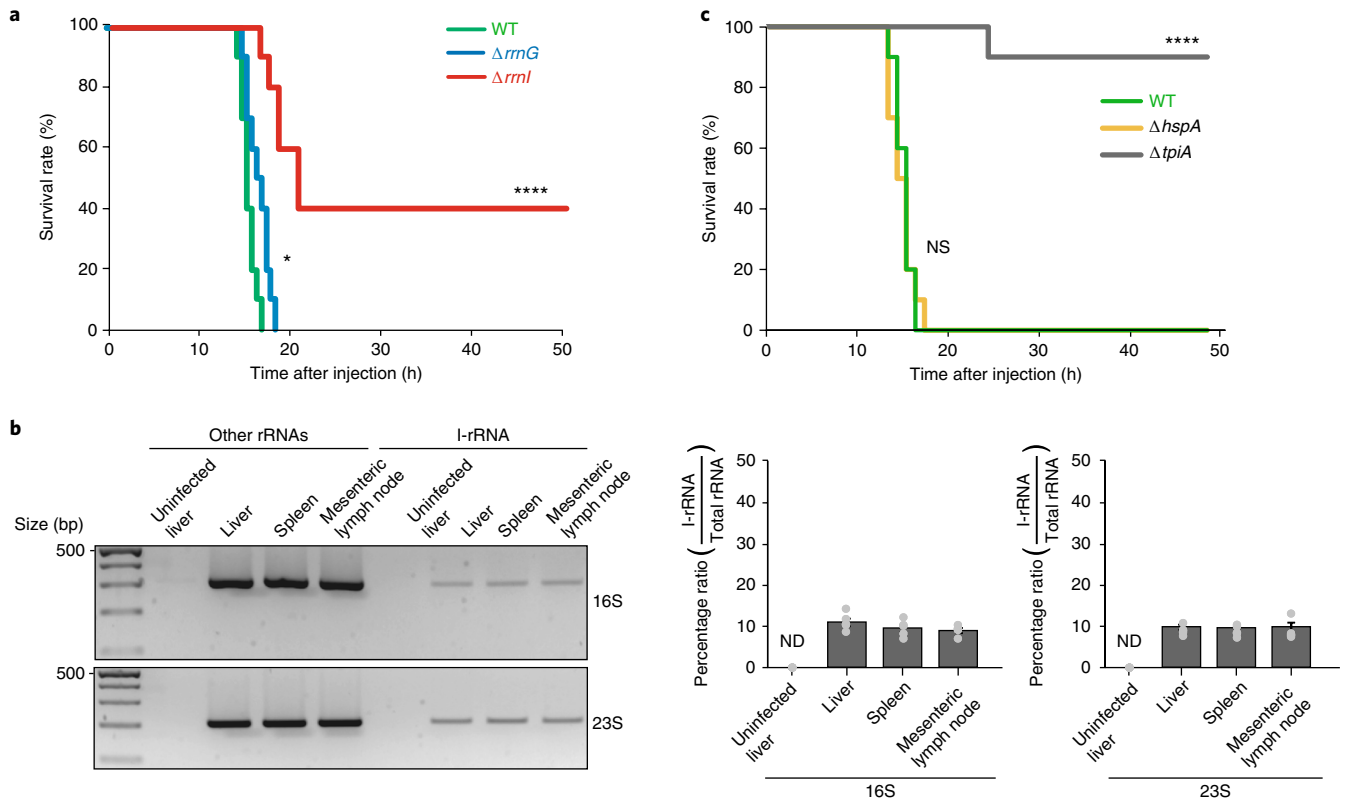

Fig. 4 | Effect of *rrnI* deletion on the virulence of *V. vulnificus* in mice. a, Survival rates and duration of survival of mice infected with *V. vulnificus* (WT, Δ*rrnG* or Δ*rrnI* strains). Pathogen-free 7-week-old female ICR mice pretreated with iron dextran ($n=10$ mice per group) were intraperitoneally injected with 8×10^2 cells of *V. vulnificus*. The survival rate was monitored for 2 days. $^*P<0.05$, $^{****}P<0.0001$ for Δ*rrnG*- or Δ*rrnI*-infected mice versus WT-infected mice (two-sided unpaired Student's *t*-test). **b**, Characterization of I-rRNA expression in WT *V. vulnificus* cells during infection. Total RNA was isolated from the liver, spleen and mesenteric lymph nodes of WT *V. vulnificus*-infected mice ($n=5$ mice), and cDNA was synthesized from the total RNA purified from each organ. The number of amplicons of 16S or 23S I-rRNAs and other 16S or 23S rRNAs amplified from the cDNAs was determined by PCR with reverse transcription (RT–PCR) as described in Supplementary Fig. 1a. The relative abundance of each group of rRNA species was quantified and is shown below the gel images. Total RNA purified from the liver of uninfected mice was used as a control for the specificity of primers. The data are presented as the mean ± s.e.m. of three independent experiments. **c**, Survival rates and duration of survival of mice infected with WT, *hspA*- or *tpiA*-deleted strains. The experiments were performed as described above for **a**. The survival rate was monitored for 2 days. $^{****}P<0.0001$ for Δ*hspA*- or Δ*tpiA*-infected mice versus WT-infected mice (two-sided unpaired Student's *t*-test).

Fig. 8a). When the secondary structures of the wild type (WT-SD1) and mutant (SD-MT1) SD sequences were analysed using RNase digestion of 5′-^{32}P-end-labelled synthetic RNAs, the generation of two large bulges in SD-MT1 by the introduction of two nucleotide substitutions in WT-SD1 was evident (Supplementary Fig. 9a,b). This indicated that the SD sequence of SD-MT1 is more accessible to the 30S subunit.

Analogous results were obtained with another mutant SD sequence (SD-MT2) containing 12 nucleotides of the 5′ UTR upstream of the start codon of *hspA*, which contains an SD sequence in an unstructured region of the mRNA (Fig. 6a). Luciferase activities from the two mutant *hspA*-RBS::*luc* constructs were ~18-fold (SD-MT1) and 12-fold (SD-MT2) higher in all the strains tested. This effect is probably due to the increased accessibility of the SD sequences of these mutant *hspA*-RBS::*luc* mRNAs to the 30S ribosomal subunit (Fig. 6a). Repression of reporter activity was partially restored in the Δ*rrnI* strain when the SD sequence was removed from the *hspA*-RBS::*luc* mRNAs (SD-MT3 and SD-MT4) (Fig. 6a).

We further investigated whether mutations occluding the SD sequence affected the I-ribosome-mediated preferential mRNA translation of another gene (*VV1_RS01065*). Expression was not significantly changed when assessed using the luciferase fusion construct (*VV1_RS01065*-RBS::*luc*) in the WT, Δ*rrnG* and Δ*rrnI* strains (Fig. 6b; Supplementary Figs. 7q and 8b). The introduction of nucleotide substitutions in a bulge containing the SD sequence (WT-SD2) in the 5′ UTR of the fusion mRNA from the *VV1_RS01065*-RBS::*luc* construct resulted in the formation of a stem–loop that buries the SD sequence in the region (MT-SD5). This effect was predicted by the M-fold program and confirmed by an in vitro cleavage analysis (Supplementary Fig. 9c). Repression of reporter activity was observed in the Δ*rrnI* strain when the mutant SD was used (Fig. 6b; Supplementary Fig. 8b).

We further tested interrelationships between the SD–ASD interaction and the I-ribosome-mediated preferential translation of target mRNAs using an altered ASD sequence (MT-ASD; 5′-AGGGA-3′), which does not recognize mRNAs with partial or complete consensus SD sequences (5′-GGAGG-3′) in *E. coli*[37] (Supplementary Fig. 10a). The 16S rRNA with the WT-ASD or MT-ASD sequence and the 23S/5S rRNAs of the *rrnI* operon were expressed from derivatives of pRK415-*rrnI* that express I-rRNAs at near endogenous levels (pRK415-*rrnI*-PD and pRK415-*rrnI*-PD-MT-ASD, respectively). The expression levels of HspA as well as the heat shock susceptibility of Δ*rrnI* cells harbouring these constructs were then measured. The results showed that when I-rRNAs with the MT-ASD sequence were expressed at near endogenous levels

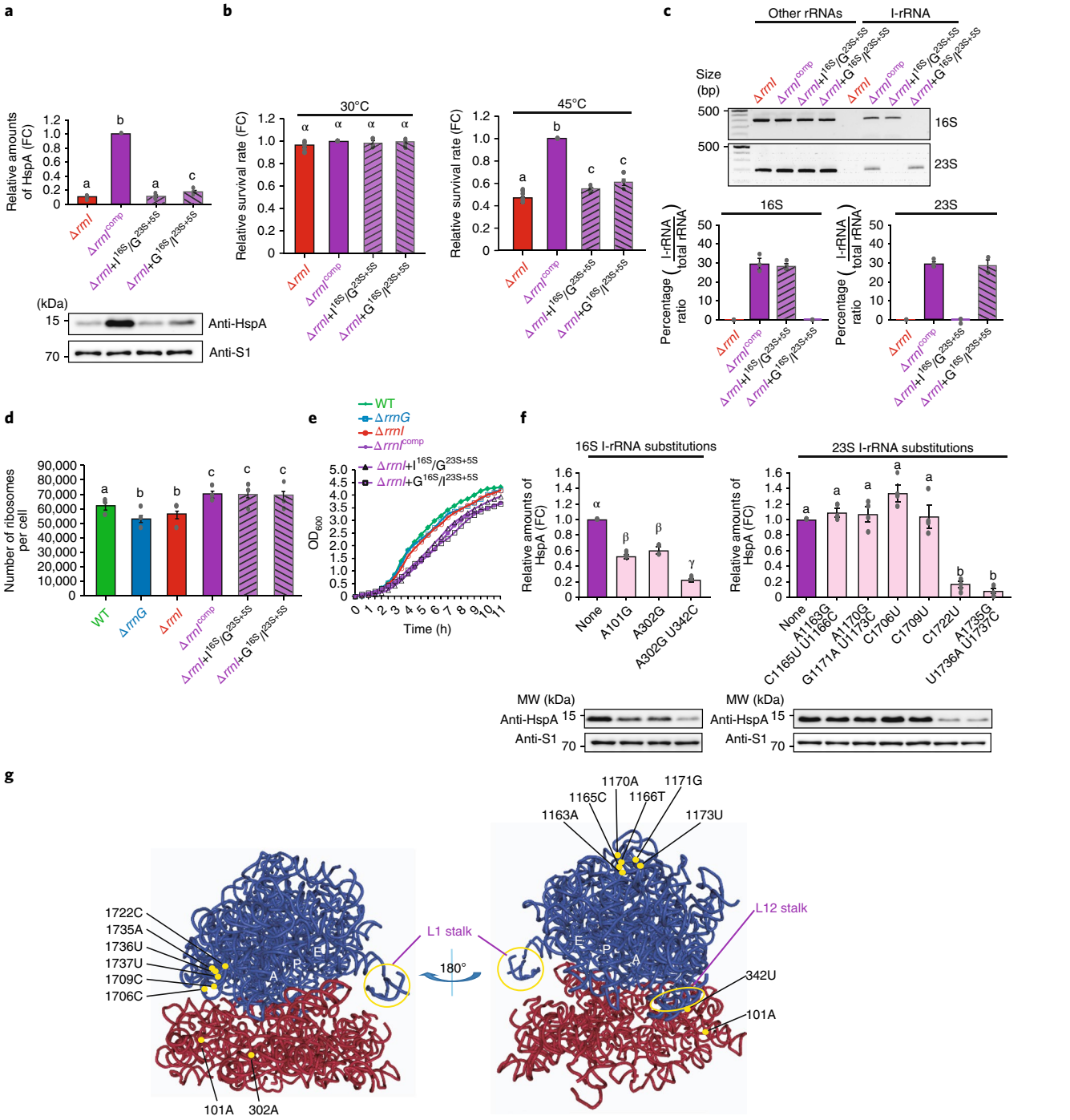

Fig. 5 | Identification of variable residues in I-rRNAs associated with *rrnI*-dependent expression of *hspA* mRNAs. a,**b**, Effects of the expression of either the 16S or the 23S/5S I-rRNAs on the translation of *hspA* mRNAs (**a**) and heat shock susceptibility (**b**) were assessed as described in the caption of Fig. 2a,b, respectively. Δ*rrnI* + I^{16S}/G^{23S+5S} and Δ*rrnI* + G^{16S}/I^{23S+5S} indicate Δ*rrnI* harbouring pRK415-I^{16S}/G^{23S+5S} and pRK415-G^{16S}/I^{23S+5S}, respectively. **c**, The expression and incorporation of I-rRNAs in the Δ*rrnI*, Δ*rrnI*^{comp}, Δ*rrnI* + I^{16S}/G^{23S+5S} and Δ*rrnI* + G^{16S}/I^{23S+5S} strains were determined by allele-specific RT–PCR as described in the caption of Supplementary Fig. 1a. The data are presented as the mean ± s.e.m. of three independent experiments. **d**,**e**, Effects of *rrnI* expression levels on the number of ribosomes per cell (**d**) and the growth of *V. vulnificus* (**e**). WT, Δ*rrnG*, Δ*rrnI*, Δ*rrnI*^{comp}, Δ*rrnI* + G^{16S}/I^{23S+5S} and Δ*rrnI* + I^{16S}/G^{23S+5S} strains were grown in LBS medium. Data are representative of three independent experiments, and similar results were obtained (**e**). **f**, Identification of variable residues in I-rRNAs responsible for the I-ribosome-dependent translation of *hspA* mRNAs. Nucleotide substitutions were introduced into the I-rRNA genes in pRK415-*rrnI*. For **a** and **f**, the expression levels of *hspA* mRNAs were not significantly changed in any of the strains (Supplementary Figs. 4c and 6a). For **a**, **b** and **f**, the expression levels of HspA (**a**, **f**) and the number of CFUs (**b**) were compared by setting those of Δ*rrnI*^{comp} to 1. The data are presented as the mean ± s.e.m. of at least three independent experiments ($n = 4$ (**a**), $n = 5$ (**b**), $n = 3$ (**d**), $n = 3$ (**f**)), and significant values are indicated by different letters (one-way ANOVA with Student–Newman–Keuls test, $P < 0.0001$; Greek symbols indicate the difference from 30 °C in **b** and 16S I-rRNA substitutions in **f**; English letters indicate the difference from 45 °C in **b** and **d**, and 23S-I rRNA substitutions in **f**). **g**, Location of the I-rRNA variable residues within the ribosome structure. The tertiary structure of the *E. coli* ribosome was obtained from Protein Data Bank (code: 3DG0). The 16S rRNA and 23S rRNA are shown in red and blue chains, respectively. The variable residues of I-rRNAs are indicated by yellow closed circles. The L1 and L12 stalks and the A, P and E sites are also indicated.

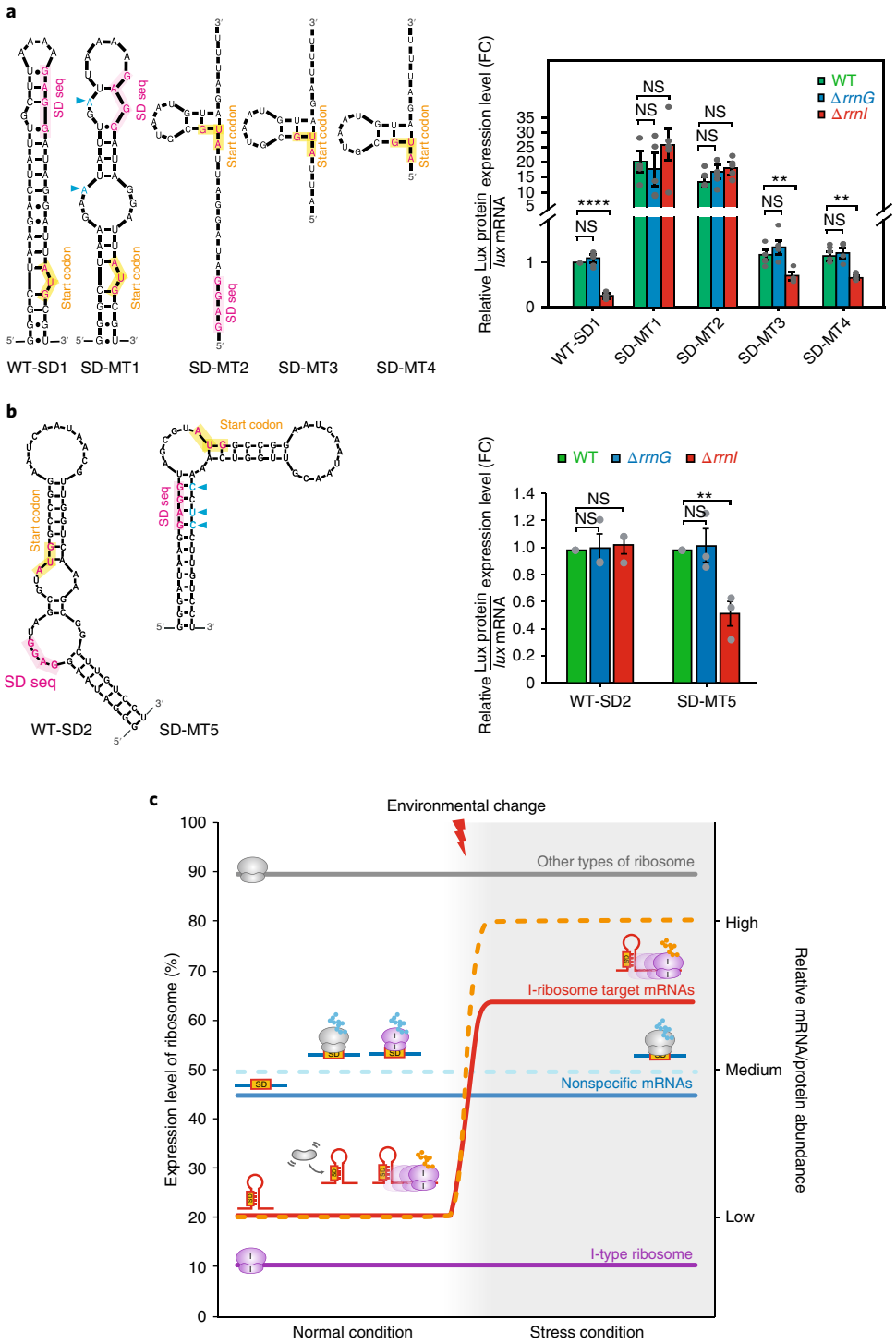

Fig. 6 | Characterization of I-ribosome-mediated preferential mRNA selection. a, Effect of SD sequence (SD seq) accessibility and availability on I-ribosome-dependent expression of *hspA*-RBS::*luc*. Left: secondary structures of the mutant *hspA*-RBS::*luc* constructs. Nucleotide substitutions (blue arrowheads) or deletions were introduced into the 5′ UTR of *hspA* to increase SD sequence accessibility (SD-MT1 and SD-MT2) or to remove the SD sequence (SD-MT3 and SD-MT4). Right: effect of structural changes in the ribosome-binding site of *hspA*-RBS::*luc* mRNA on I-ribosome-dependent translation. **b**, Effect of SD sequence accessibility on I-ribosome-independent expression of *VV1_RS01065*-RBS::*luc*. Left: secondary structures of the WT and mutant *VV1_RS01065*-RBS::*luc* constructs. Nucleotide substitutions (blue arrows) were introduced into the 5′ UTR of *VV1_RS01065* to decrease SD sequence accessibility (SD-MT5). Right: effect of structural changes in the ribosome-binding site of *VV1_RS01065*-RBS::*luc* mRNA on I-ribosome-independent translation. The luciferase activity of various *V. vulnificus* strains harbouring mutant fusion constructs was assessed as described in the caption of Fig. 1b. Luciferase activities were normalized using the *lux* reporter mRNA levels shown in Supplementary Fig. 8. The expression levels of *lux* mRNA were compared by setting those of the WT to 1. The data are presented as the mean ± s.e.m. of five (**a**) or three (**b**) independent experiments. $^{**}P < 0.01$, $^{****}P < 0.0001$ (two-sided unpaired Student's *t*-test). **c**, Schematic representation of a model of I-ribosome-mediated differential protein synthesis in *V. vulnificus*. I-ribosomes target mRNAs with 5′ UTR structures that obscure the SD sequence, thus binding and translating target mRNAs coding for stress response proteins. Under stress conditions, I-ribosome-mediated preferential translation of target mRNAs with induced expression levels results in enhanced protein production from target mRNAs. This mechanism helps *V. vulnificus* cells adapt to environmental changes. Dotted and solid lines indicate abundance of protein and mRNA, respectively.

(~12% of total rRNAs) in Δ*rrnI* cells (Δ*rrnI*^{comp}-PD + MT-ASD), the expression levels of HspA decreased by ~45% compared with those in Δ*rrnI* cells harbouring pRK415-*rrnI*-PD (Δ*rrnI*^{comp}-PD) and increased by nearly 4.6-fold compared with those in Δ*rrnI* cells (Supplementary Fig. 10b,c). The expression levels of HspA in Δ*rrnI*^{comp}-PD + MT-ASD cells decreased by ~24% compared with those in WT cells (Supplementary Fig. 10c,d). This restored the heat shock susceptibility of Δ*rrnI* cells to levels comparable to those in WT and Δ*rrnI*^{comp}-PD cells (Supplementary Fig. 10e).

Taken together, these results indicate that the I-ribosome does not heavily rely on the SD–ASD interaction to preferentially select *hspA* mRNAs. In addition, consistent with the results presented in Fig. 5, these results show that I-ribosome-mediated preferential translation of target mRNAs is unlikely to be due to the overexpression of I-rRNAs.

Discussion

As highlighted in this study, a subpopulation of ribosomes containing genome-encoded divergent rRNAs (I-ribosomes) directs the preferential translation of a subset of mRNAs. In this case, a dramatic change in ribosomal protein composition is unlikely to be involved in preferential mRNA selection. This is because no significant differences in the stoichiometry of the ribosomal proteins were observed when the relative abundance of ribosomal proteins from 70S ribosomes purified from WT, Δ*rrnI* and Δ*rrnI*^{comp} cells was assessed using MS with TMT technology. This procedure successfully quantified 53 out of 54 ribosomal proteins (Supplementary Fig. 10f). Conventional interactions between SD and ASD sequences also do not seem to play a critical role in the I-ribosome-mediated preferential mRNA selection (Fig. 6a,b; Supplementary Fig 10a–e). However, the presence of both ribosomal subunits containing I-rRNAs is required (Fig. 5). Although our results do not indicate a strong association between I-ribosome-mediated mRNA selection and the SD–ASD interaction, I-ribosome target mRNAs are unlikely to be limited to those that are poorly translated (Supplementary Fig. 11). This mode of mRNA selection is not unusual. Indeed, additional examples of unconventional mRNA selection mechanisms include translation initiation by a synthetic ribosome with tethered subunits[38], translation initiation of leaderless mRNAs by 70S ribosomes[24,39] and translation by scanning re-initiation[40]. Further studies are needed to reveal the detailed mechanism of I-ribosome-mediated preferential mRNA selection.

The expression of I-rRNAs is not predicted to be regulated differently from that of other rRNAs, since the promoter region of the *rrnI* operon is highly similar to that of the other *rrn* operons (Supplementary Fig. 12). In agreement with this observation, the proportion of I-ribosomes did not significantly change during heat shock (Supplementary Fig. 13a), whereas the levels of *hspA* mRNA and HspA protein increased by ~2.5-fold and 10-fold, respectively (Supplementary Fig. 13b,c). On the basis of our results, we propose a model for I-ribosome action whereby relatively constant cellular levels of I-ribosomes enhance protein synthesis from target mRNAs that are upregulated under specific conditions. This process contributes to the adaptation of *V. vulnificus* to environmental changes such as variations in temperature and nutrient availability (Fig. 6d). This would probably explain why *V. vulnificus* still possesses divergent rRNA genes, despite the general flow of evolution that has led to the convergence of rRNA genes in most organisms. Similar to what had been previously shown for heterogeneous rRNAs generated by sequence-specific cleavage of endoribonucleases[22,24,28], this study demonstrates that genome-encoded divergent rRNAs are able to reprogramme ribosomes to have specialized activity. Remarkably, results from this study and other studies indicate that rRNA heterogeneity, regardless of how it is generated, converts the protein synthesis machinery into a regulatory hub that modulates the cellular proteomic profile in response to environmental cues. Therefore, rRNA heterogeneity might be a mechanism of stress adaptation in bacteria[21,22,24,28]. In addition, recent studies have reported that genome-encoded divergent rRNAs are required for halophilic archaea *Haloarcula* species to grow optimally at high temperatures[19,20]. In this regard, it is interesting to note that significant differences in the sequences of genome-encoded rRNAs have been observed in many organisms that live in physically extreme or host environmental conditions or have a developmentally complex life cycle[14].

Methods

Animals. Pathogen-free 7-week-old female ICR mice ($n = 10$) were purchased from Orient Bio and kept in isolated cages in a barrier animal facility with a 12-h light–dark cycle in a temperature-controlled (22 ± 1 °C) room at Chung-Ang University. Mice were fed ad libitum with a regular diet. The experiment was conducted as a completely randomized design, and the analyses were performed in a blinded manner. No statistical methods were used to determine mouse sample sizes.

Bacterial strains and plasmid construction. *V. vulnificus* strains were grown at 30 °C in LBS medium or at 37 °C in minimal medium (50 mM Na_2HPO_4, 20 mM KH_2PO_4, 0.5 M NaCl, 5 mg per litre thiamine-HCl, 1 mM NH_4Cl, 2 mM $MgCl_2$) containing 20 mM glucose (glucose medium) or 40 mM glycerol (glycerol medium) as a carbon source. *E. coli* strains were grown in Luria–Bertani (LB) medium at 37 °C.

The bacterial strains, plasmids and primers used in this study are listed in Supplementary Tables 6 and 7. Δ*rrnG*, Δ*rrnI*, Δ*hspA* and Δ*tpiA* were constructed using the homologous recombination method[41]. The 5′ UTR and 3′ UTR of each gene were amplified using *V. vulnificus* CMCP6 genomic DNA as a template, and were assembled by overlap extension PCR[42]. The kanamycin resistance gene (*nptI*) was obtained by digestion of pUC4K with PstI. The resulting fragment was cloned into the pSD80 plasmid using EcoRI, PstI and XbaI, and was subcloned into the suicide vector pDM4 using XbaI and SacI. The pDM4 plasmid containing the deletion cassette was conjugated into *V. vulnificus* CMCP6, in which allelic homologous recombination took place.

To construct pRK415-*rrnI*, the *rrnI* operon with its putative promoter was amplified from *V. vulnificus* CMCP6 genomic DNA using primers rrnI 5′-UTR-400 EcoRI-F, rrnI 16S XbaI-R, rrnI 23S XbaI-F and rrnI 23S PstI-R, and was ligated into the EcoRI/XbaI and XbaI/BamHI sites of pRK415 (Supplementary Table 6). To construct the chimeric and mutant rRNA genes, the 16S rRNA and 23S/5S rRNA regions were amplified using *V. vulnificus* CMCP6 genomic DNA as a template and were cloned into pRK415-*rrnI*. To clone the putative *rrnI*-target gene into pBBR-lux, a 20-amino-acid-long coding region or the entire CDS with its putative promoter was amplified from *V. vulnificus* CMCP6 genomic DNA and was ligated into the SpeI and BamHI sites of pBBR-lux. To construct pBBR-lux-SD MTs, the PCR products amplified were cloned into the SpeI and BamHI sites of pBBR-lux. To generate a base substitution in the −10 box of the *rrnI* promoter in pRK415-*rrnI* or pRK415-*rrnI*-MT-ASD, the PCR products amplified were cloned into the plasmid using the BglII and EcoRI sites of pRK415-*rrnI* and pRK415-*rrnI*-MT-ASD, resulting in pRK415-*rrnI*-PD and pRK415-*rrnI*-PD-MT-ASD, respectively.

Isolation of total RNA and 70S ribosomes. The 70S ribosomes were isolated as previously described[43,44]. In brief, cells grown to mid-log phase were lysed with a French press. The lysate was then loaded onto a 30% sucrose cushion. Crude ribosomes were pelleted by centrifugation at 100,000*g* for 16 h at 4 °C. The pellet was resuspended and loaded onto a 15–40% sucrose gradient and centrifuged at 79,500*g* for 13.5 h at 4 °C. After centrifugation, 70S ribosomes were obtained by fractionation and measurement of the optical density (OD) at 260 nm.

Quantification of I-rRNA distribution. The distribution of 16S or 23S I-rRNAs in ribosomes was determined by allele-specific RT–PCR and a modified primer extension method[37] (Supplementary Fig. 1). rRNAs were purified from 70S ribosomes by phenol–chloroform extraction followed by ethanol precipitation. For the amplification of I-rRNAs for allele-specific RT–PCR, complementary DNA was synthesized using an iScript cDNA synthesis kit (Bio-Rad Laboratories) according to the manufacturer's instructions. Primers specific for 16S or 23S *rrnI* were designed with a mismatch at the position of the variable nucleotide (Supplementary Table 1). PCR cycling was performed using the following parameters: an initial denaturation step at 95 °C for 3 min; then 39 cycles of 95 °C for 30 s, 64 °C for 30 s, and 72 °C for 40 s; and a final extension step at 72 °C for 5 min. PCR products were separated on a 1.5% agarose gel by electrophoresis and visualized under ultraviolet light. For the modified primer extension method, the primer (rrnI-23S rRNA-1743R; complementary to nucleotides 1743–1762 of the 23S rRNA) was labelled at the 5′-end using [γ-^{32}P]ATP and T4 polynucleotide kinase (New England Biolabs). RNA and labelled primers were annealed at 65 °C for 5 min, and the reaction was then cooled to 37 °C. The extension reaction was catalysed by AMV reverse transcriptase (New England Biolabs) at 42 °C for 1 h.

The extended fragments were separated on a 10% polyacrylamide-8 M urea-TBE gel and visualized on a phosphoimager.

Ribosome profiling analysis of ribosome-protected mRNA fragments. The procedure for ribosome profiling has been described previously[45]. Δ*rrnI* and Δ*rrnI*^{comp} cells were grown at 30 °C in LBS media containing 0.2 μg ml^{-1} tetracycline to an OD_{600} of 0.7. After treatment with 100 μg ml^{-1} chloramphenicol to stop translation, the cells were incubated at 30 °C for 5 min. The culture was cooled on ice and collected by centrifugation. The pellet was washed with prechilled buffer A (50 mM Tris-HCl, pH 7.6, 10 mM $MgCl_2$, 100 mM NH_4Cl, 6 mM 2-mercaptoethanol, 0.5 mM EDTA) containing 1 mM of chloramphenicol and was lysed using a French press. Cellular debris was removed by centrifuging for 30 min at 30,000*g*. The clarified lysate (supplemented with 5 mM $CaCl_2$) was digested with micrococcal nuclease for 1 h at 25 °C and quenched with EGTA to a final concentration of 6 mM. The resulting lysate was loaded onto a 30% sucrose cushion. Crude ribosomes were pelleted by centrifugation at 100,000*g* for 16 h at 4 °C. The pellets were resuspended and loaded onto a 15–40% sucrose gradient and centrifuged at 79,500*g* for 13.5 h at 4 °C. After centrifugation, monosomes were obtained by fractionation and measurement of optical density at 260 nm. Monosomal RNA was obtained by phenol extraction and ethanol precipitation and was resuspended in RNase-free water. To obtain ribosome-protected mRNAs, extracted monosomal RNA was resolved on a 15% polyacrylamide-8 M urea-TBE gel. A band between 28 and 42 base pairs was excised, gel purified, precipitated and resuspended in RNase-free water. For ribosomal RNA depletion, a Ribo-Zero rRNA Removal kit (Illumina) was used according to the manufacturer's instructions. Isolated RNAs were used to construct a cDNA library for Illumina sequencing using a TruSeq Small RNA Sample Prep kit (Illumina) according to the manufacturer's instructions. RNA sequencing was performed by Chunlab on an Illumina MiSeq and HiSeq 2500 platform using single-end 50-bp sequencing.

Transcriptome analysis. Total cellular RNA was extracted from cultures of Δ*rrnI* and Δ*rrnI*^{comp} cells grown at 30 °C in LBS media containing 0.2 μg ml^{-1} tetracycline to an OD_{600} of 0.7 using TRIzol (Thermo Fisher Scientific) according to the manufacturer's instructions. The mRNA in total RNA was converted into a library of template molecules suitable for subsequent cluster generation using the reagents provided in the Illumina TruSeq RNA Sample Preparation kit (Illumina). The first step in the workflow involved removing the rRNA in the total RNA using the Ribo-Zero rRNA Removal kit (Illumina). Following this step, the remaining mRNA was fragmented into small pieces using divalent cations under elevated temperature. The cleaved RNA fragments were copied into first strand cDNA using reverse transcriptase and random primers. This was followed by second strand cDNA synthesis using DNA Polymerase I and RNase H. These cDNA fragments then underwent an end repair process, the addition of a single 'A' base, and then ligation of the adapters. The products were then purified and enriched by PCR to create the final cDNA library. RNA sequencing was performed by Chunlab on an Illumina HiSeq 2500 platform using single-end 50-bp sequencing.

RNA sequencing data analysis. Single-end reads were mapped onto the reference genome sequence (NCBI Biosample ID: SAMN02603130) using BWA (v.0.7.17)[46]. Coordinates of genome features such as protein coding genes were extracted from the NCBI genome annotation information. Numerical count data were transformed into reads per kilobase per million mapped reads (RPKM) to normalize for the number of sequencing reads and total read length[47]. An RPKM cut-off value of 30 was applied to filter the abundance data. Transcriptome analysis data were used for normalization of the ribosome profiling analysis data for mRNA abundance, and the resulting data were used to assess fold changes in the nRFP in the Δ*rrnI*^{comp} strain versus those in the Δ*rrnI* strain. Genes with a fold change of greater than 1.5 were selected for further study. The statistical differences in translational efficiency between Δ*rrnI*^{comp} and Δ*rrnI* samples were determined using nonparametric (NOIseq, probability of >0.7) (v.2.8.0)[48] approaches in the R Bioconductor package (http://www.bioconductor.org) (v.3.1.2).

Global proteome quantification. The relative abundance of total cellular proteins was quantified by iTRAQ labelling. Cells were resuspended in 95 °C pre-heated SDT-lysis buffer containing 100 mM Tris, pH 7.6, 100 mM dithiothreitol and 5% (w/v) SDS using 1:10 sample to buffer ratio[49]. The lysates were heated for 10 min at 95 °C followed by sonication for 15 min to achieve complete lysis and further processed by the filter-aided sample preparation (FASP) method[50]. Briefly, the sample was loaded onto an Amicon centrifugal filter with a 10-kDa cut-off (Merck). The proteins were alkylated using 40 mM chroloacetamide followed by overnight digestion at 37 °C with a Lys-C (Wako) and trypsin (Promega) mixture in 50 mM ammonium bicarbonate (ABC) at an enzyme to protein ratio of 1:100 (w/w). Peptides were collected from the filter after centrifugation and eluted with 50 mM ABC twice. Total peptide concentration was measured using a Quantitative Colormetric Peptide Assay (Thermo Fisher Scientific) following the manufacturer's protocol, and 80 μg peptides of each sample was dried in vacuo. Peptides were labelled using six isobaric labelling reagents (113 to 118) in iTRAQTM 8-plex reagent for 2 h according to the manufacturer's instructions. The labelling reaction was quenched with 300 μl of 0.05% trifluoroacetic acid (TFA). The samples were then combined, speed-vacuum dried and resuspended in 1% TFA. The iTRAQ-labelled peptide mixture was fractionated on STAGE-Tips[51] by strong anion exchange chromatography[52] and reverse-phase chromatography using a stepwise gradient of increasing acetonitrile (5, 7.5, 10, 12.5, 15, 20 and 80%) in 2.5 mM ABC[53]. The resulting 13 fractions were analysed by liquid chromatography with MS/MS.

MS analysis for proteome quantification. All spectra from iTRAQ-labelled peptide samples were acquired on a Q-Exactive mass spectrometer (Thermo Fisher Scientific) coupled to an EASY-nLC 1000 (Thermo Fisher Scientific). Peptides were separated on a 15-cm reversed phase analytical column (75-μm internal diameter) packed in-house with ReproSil-Pur C18-AQ 3-μm resin (Dr. Maisch) using a 120 min gradient from 5% to 35% solvent B (90% acetonitrile, 0.1% formic acid) at a flow rate of 350 nl min^{-1}. The mass spectrometer was operated in the data-dependent mode to automatically switch between full-scan MS1 and MS2 acquisition. Survey full scan MS1 spectra were acquired for mass range 300–1,800 *m*/*z* with an automatic gain control target of 3e6 ions, a resolution of 70,000 and maximum injection time of 120 ms. The top 12 most intense MS1 ions were isolated for MS2 analysis. After 5e5 ions were accumulated, ions were fragmented by high-energy collision-induced dissociation (normalized collision energy, 27%, isolation width, 2 *m*/*z*). The *m*/*z* of fragmented ions were measured with a resolution of 17,500 and maximum injection time of 60 ms.

The raw files were processed using MaxQuant v.1.6.1.0[54]. The MS/MS spectra were searched against the NCBI reference sequence (NC_04459.3, NC_004460.2) and UniProt YJ016 proteome databases (4 February 2017 release) with precursor and fragment ion mass errors set to 4.5 ppm and 20 ppm, respectively, and with up to two missed cleavages. Modifications at the amino terminus and lysine residues caused by the iTRAQ reagent and carbamidomethylation of cysteine were set as fixed modifications, and oxidation of methionine was chosen as a variable modification for database searching. The reporter mass tolerance was set to 0.001 Da around the theoretical mass value. Both peptide and protein identifications were filtered at a 1% false discovery rate. The cellular proteome dataset was normalized using the quantile normalization method[55]. Statistical differences between groups were calculated using Student's *t*-test, with a *P* value below 0.05 considered statistically significant. Bioinformatics analyses and visualization were performed using Perseus 1.6.1.1[56].

Bioluminescence assays. Bioluminescence assays were performed as described previously[57]. In brief, a pBBR-lux cassette was conjugated into *V. vulnificus* WT, Δ*rrnG* and Δ*rrnI* strains. Cells were grown in LBS medium at 30 °C overnight, and cultures were diluted at a ratio of 1:100 in LBS medium. The relative lux levels for each strain were measured when the OD_{600} reached 0.6–0.7, and the relative light units were calculated.

Isolation of total RNA and quantitative rtPCR. Total cellular RNA was extracted from cultures grown to an OD_{600} of 0.6 using a RNeasy mini prep kit (Qiagen). Following confirmation of the quality and quantity of the extracted total RNA with a Nanodrop 2000 instrument (Thermo Fisher Scientific), cDNA was synthesized using an iScript cDNA Synthesis kit (Bio-Rad Laboratories). Samples for quantitative rtPCR were prepared to a final volume of 10 μl using Applied Biosystems SYBR green PCR master mix (Bio-Rad Laboratories). Quantitative rtPCR was performed on a CFX-96 Thermal Cycler and Detection System (Bio-Rad Laboratories).

Antibody purification and western blot analysis. Polyclonal antibodies against HspA and TpiA were obtained from rabbits inoculated with purified His-tagged HspA and TpiA. *V. vulnificus* HspA and TpiA were purified from *E. coli* DH5α strains containing pKAN6B-HspA-His and pKAN6B-TpiA-His, respectively, using Ni-NTA agarose (Qiagen). The proteins were eluted from columns using 250 mM imidazole, concentrated and stored as described previously[58]. Antibodies were purified using AminoLink Plus Immobilization kits (Thermo Fisher Scientific) according to the manufacturer's instructions.

The proteins were resolved on a 12% SDS polyacrylamide gel, and the gels were electroblotted onto a nitrocellulose membrane. Images of the western blots were obtained using an Amersham Imager 600 (GE Healthcare) and were quantified using Quantity One (Bio-Rad Laboratories). The ribosomal protein S1 was used as the control.

Measurement of heat shock susceptibility. *V. vulnificus* strains were grown in LBS medium containing 0.2 μg ml^{-1} tetracycline at 30 °C until reaching an OD_{600} of 0.6, and 500 μl of each culture was immediately incubated for 3 h in a water bath at 45 °C. The non-heated and heated cultures were serially diluted in LBS medium, and aliquots containing 10^{-5} and 10^{-6} cells were spread onto LBS-agar plates containing 0.2 μg ml^{-1} tetracycline. The plates were incubated at 30 °C for 16 h, and the colonies were counted.

Analysis of growth characteristics on minimal medium. Cells were grown at 37 °C in LBS medium overnight, after which 1 ml was collected and washed twice with 1 volume of minimal medium. One-fiftieth of the washed cells was reinoculated into 2 ml of minimal medium and incubated overnight. Then, the OD_{600} of the culture was adjusted to 0.1, and the cells were incubated for 2 h in minimal medium to eliminate any remaining source of rich medium. The culture was then washed, used to inoculate 50 ml of minimal medium, and incubated at 37 °C. Cell growth was monitored by measuring the cell density (OD_{600}) at the indicated time points.

Methylglyoxal assay. Cells were grown at 37 °C in LBS medium containing 0.2 μg ml^{-1} tetracycline. After 24 h, cells were collected and washed twice with 1 volume of glycerol medium containing 0.2 μg ml^{-1} tetracycline and were grown in 30 ml of glycerol medium containing 0.2 μg ml^{-1} tetracycline at 37 °C. After 24 h, the cells were washed twice with 1 volume of glycerol medium and reinoculated into 2 ml of fresh glycerol medium containing 0.2 μg ml^{-1} tetracycline (OD_{600} = 2.0). Inoculated cells were further incubated at 37 °C, and samples were collected 48 h after re-inoculation. The methylglyoxal concentration in the medium was determined as described previously[59].

Mouse mortality test. *V. vulnificus* WT, Δ*rrnG* and Δ*rrnI* strains were grown in LBS medium to mid-log phase, and aliquots containing 8×10^3 cells per ml were taken and washed in PBS buffer. Before injection, pathogen-free, 7-week-old female ICR mice (n = 10) were fasted for 24 h and deprived of water for 4 h. Iron dextran (80 μg per g body weight) was injected intraperitoneally into the mice. After 1 h, *V. vulnificus* WT, Δ*rrnG* or Δ*rrnI* cells were injected intraperitoneally at a concentration of 8×10^2 cells in 100 μl PBS into each mouse. Mice were monitored for 48 h, and dead mice were counted.

Isolation of total RNA from organs of *V. vulnificus*-infected mice. A group of five mice (7-week-old females) was infected via intraperitoneal administration with 8×10^2 CFUs of the WT strain in 100 μl of PBS. Mice were killed at 12 h post-infection, and the spleen, liver and mesenteric lymph nodes were removed aseptically and homogenized in 500 μl of ice-cold TRIzol (Thermo Fisher Scientific). Total RNA samples were purified by phenol extraction and ethanol precipitation.

Assessment of number of bacterial cells and number of ribosomes per cell. For measurement of bacterial cell counts, WT, Δ*rrnG*, Δ*rrnI*, Δ*rrnI*^{comp}, Δ*rrnI* + G^{16S}/I^{23S+5S} and Δ*rrnI* + I^{16S}/G^{23S+5S} strains were grown in LBS medium to mid-log phase. The cultures were diluted in PBS and analysed using a BD Accuri C6 Plus flow cytometer (BD Biosciences). Crude ribosomes were isolated from the cultures as described above and used for assessing the number of ribosomes per cell based on one unit of A_{260} corresponding to 23 pmol of 70S ribosome.

In vitro synthesis of RNA and cleavage assay. Synthetic RNAs containing WT-SD1, SD-MT1, WT-SD1-short, SD-MT1-short, WT-SD2 or MT-SD5 were synthesized from PCR DNA products using a MEGAshortscript T7 kit (Thermo Fisher Scientific) according to the manufacturer's instructions. The PCR DNA products were amplified from pBBR-lux-VV1_RS04755, pBBR-lux-SD MT1, pBBR-lux-VV1_RS01065 and pBBR-lux-SD MT5 respectively, using the following primers: VV1_RS04755-T7-F and VV1_RS04755-20aa-R; VV1_RS04755-T7-short-F and VV1_RS04755-6aa-R; or VV1_RS01065 T7-cleavage F and VV1_RS01065 T7-cleavage R. The RNAs were purified and 5′-^{32}P-end-labelled as described previously[60]. One picomole of 5′-^{32}P-end-labelled RNA was incubated with 2.5 U of RNase T1 and 100 pg of RNase A in cleavage buffer (50 mM Tris-Cl, pH 8, 100 mM NaCl) at 37 °C. Samples were withdrawn at the indicated time points and separated on 12% polyacrylamide gel containing 8 M urea.

Ribosomal protein quantification. The relative abundance of ribosomal proteins in purified 70S ribosomes was quantified by iTRAQ labelling. Ribosomal proteins were purified from the 70S ribosomes using TRIzol (Thermo Fisher Scientific) according to the manufacturer's instructions. The ribosomal protein mixtures were dissolved in SDT-lysis buffer, followed by incubation at 95 °C for 10 min, and were further processed using the FASP method. Briefly, the sample was loaded on an Amicon centrifugal filter with a 10-kDa cut-off (Merck Millipore). The proteins were alkylated by 40 mM chroloacetamide, followed by overnight digestion at 37 °C with Lys-C (Wako) and trypsin (Promega) in 50 mM ABC at an enzyme to protein ratio of 1:100 (w/w). Peptides were collected from the filter after centrifugation and eluted twice with 50 mM ABC. Total peptide concentration was measured using a Quantitative Colorimetric Peptide Assay (Thermo Fisher Scientific) following the manufacturer's protocol. Then, 80 μg of peptide from each sample was labelled using iTRAQ 8-plex reagent (AB Sciex) according to the manufacturer's instructions. After 2 h of labelling at room temperature, the reaction was quenched with 300 μl of 0.05% TFA. The samples were then combined, speed-vacuum dried, and resuspended in 1% TFA. The iTRAQ-labelled peptide mixture was desalted and fractionated on STAGE-Tips by reverse-phase chromatography using a stepwise gradient of increasing acetonitrile (5, 7.5, 10, 12.5, 15, 20 and 80%) in 2.5 mM ABC. The resulting seven fractions were analysed by liquid chromatography with MS/MS.

Quantification and statistical analyses. All statistical details of experiments are included in the figure legends. Multiple comparison analyses of values were performed using SAS v.9.2 with the Student–Newman–Keuls test (SAS Institute), and the Student's *t*-test was used for comparisons with controls using SAS v.9.2 and SigmaPlot (Systat Software). The data are presented as the mean ± s.e.m., and $P < 0.05$ was considered to indicate statistical significance. See Supplementary Table 8 for exact statistics and reproducibility.

Ethics statement. All animal experimental protocols of the study were performed in accordance with the national guidelines for the use of animals in scientific research and were approved by Chung-Ang University Support Center (appproval no. CAU2012-0044).

Reporting Summary. Further information on research design is available in the Nature Research Reporting Summary linked to this article.

Data availability

Ribosome profiling and transcriptome data have been deposited into the Gene Expression Ominbus (GEO) and are available under identifier GSE111991. Proteome data have been deposited into PRIDE and are available via ProteomeXchange under identifier PXD009215.

Received: 13 July 2018; Accepted: 5 December 2018;
Published online: 4 February 2019

References

1. Noller, H. F. Evolution of protein synthesis from an RNA world. *Cold Spring Harb. Perspect. Biol.* **4**, a003681 (2012).
2. Klappenbach, J. A., Saxman, P. R., Cole, J. R. & Schmidt, T. M. rrndb: the Ribosomal RNA Operon Copy Number Database. *Nucleic Acids Res.* **29**, 181–184 (2001).
3. Long, E. O. & Dawid, I. B. Repeated genes in eukaryotes. *Annu. Rev. Biochem.* **49**, 727–764 (1980).
4. Hashimoto, J. G., Stevenson, B. S. & Schmidt, T. M. Rates and consequences of recombination between rRNA operons. *J. Bacteriol.* **185**, 966–972 (2003).
5. Boucher, Y., Douady, C. J., Sharma, A. K., Kamekura, M. & Doolittle, W. F. Intragenomic heterogeneity and intergenomic recombination among haloarchaeal rRNA genes. *J. Bacteriol.* **186**, 3980–3990 (2004).
6. Carranza, S., Giribet, G., Ribera, C., Baguna & Riutort, M. Evidence that two types of 18S rDNA coexist in the genome of *Dugesia* (Schmidtea) *mediterranea* (Platyhelminthes, Turbellaria, Tricladida). *Mol. Biol. Evol.* **13**, 824–832 (1996).
7. Gunderson, J. H. et al. Structurally distinct, stage-specific ribosomes occur in *Plasmodium*. *Science* **238**, 933–937 (1987).
8. Kim, H. L. et al. Expression of divergent LSU rRNA genes in the *Vibrio vulnificus* CMCP6 genome during both infection and non-pathogenic stages. *Curr. Microbiol.* **62**, 133–138 (2011).
9. Mashkova, T. D. et al. The primary structure of oocyte and somatic 5S rRNAs from the loach *Misgurnus fossilis*. *Nucleic Acids Res.* **9**, 2141–2151 (1981).
10. Parks, M. M. et al. Variant ribosomal RNA alleles are conserved and exhibit tissue-specific expression. *Sci. Adv.* **4**, eaao0665 (2018).
11. Wang, Y., Zhang, Z. & Ramanan, N. The actinomycete *Thermobispora bispora* contains two distinct types of transcriptionally active 16S rRNA genes. *J. Bacteriol.* **179**, 3270–3276 (1997).
12. Yap, W. H., Zhang, Z. & Wang, Y. Distinct types of rRNA operons exist in the genome of the actinomycete *Thermomonospora chromogena* and evidence for horizontal transfer of an entire rRNA operon. *J. Bacteriol.* **181**, 5201–5209 (1999).
13. Locati, M. D. et al. Expression of distinct maternal and somatic 5.8S, 18S, and 28S rRNA types during zebrafish development. *RNA* **23**, 1188–1199 (2017).
14. Pei, A. Y. et al. Diversity of 16S rRNA genes within individual prokaryotic genomes. *Appl. Environ. Microbiol.* **76**, 3886–3897 (2010).
15. Vetrovsky, T. & Baldrian, P. The variability of the 16S rRNA gene in bacterial genomes and its consequences for bacterial community analyses. *PLoS ONE* **8**, e57923 (2013).
16. Waters, A. P., Syin, C. & McCutchan, T. F. Developmental regulation of stage-specific ribosome populations in *Plasmodium*. *Nature* **342**, 438–440 (1989).
17. Velichutina, I. V., Rogers, M. J., McCutchan, T. F. & Liebman, S. W. Chimeric rRNAs containing the GTPase centers of the developmentally regulated ribosomal rRNAs of *Plasmodium falciparum* are functionally distinct. *RNA* **4**, 594–602 (1998).
18. van Spaendonk, R. M. et al. Functional equivalence of structurally distinct ribosomes in the malaria parasite, *Plasmodium berghei*. *J. Biol. Chem.* **276**, 22638–22647 (2001).

19. Lopez-Lopez, A., Benlloch, S., Bonfa, M., Rodriguez-Valera, F. & Mira, A. Intragenomic 16S rDNA divergence in *Haloarcula marismortui* is an adaptation to different temperatures. *J. Mol. Evol.* **65**, 687–696 (2007).
20. Sato, Y., Fujiwara, T. & Kimura, H. Expression and function of different guanine-plus-cytosine content 16S rRNA genes in *Haloarcula hispanica* at different temperatures. *Front. Microbiol.* **8**, 482 (2017).
21. Kurylo, C. M. et al. Endogenous rRNA sequence variation can regulate stress response gene expression and phenotype. *Cell Rep.* **25**, 236–248 (2018).
22. Zhang, J. J., Zhang, Y. L., Zhu, L., Suzuki, M. & Inouye, M. Interference of mRNA function by sequence-specific endoribonuclease PemK. *J. Biol. Chem.* **279**, 20678–20684 (2004).
23. Shine, J. & Dalgarno, L. The 3′-terminal sequence of *Escherichia coli* 16S ribosomal RNA: complementarity to nonsense triplets and ribosome binding sites. *Proc. Natl Acad. Sci. USA* **71**, 1342–1346 (1974).
24. Vesper, O. et al. Selective translation of leaderless mRNAs by specialized ribosomes generated by MazF in *Escherichia coli*. *Cell* **147**, 147–157 (2011).
25. Culviner, P. H. & Laub, M. T. Global analysis of the *E. coli* toxin MazF reveals widespread cleavage of mRNA and the inhibition of rRNA maturation and ribosome biogenesis. *Mol. Cell* **70**, 868–880 (2018).
26. Mets, T. et al. Fragmentation of *Escherichia coli* mRNA by MazF and MqsR. *Biochimie* **156**, 79–91 (2018).
27. Tock, M. R., Walsh, A. P., Carroll, G. & McDowall, K. J. The CafA protein required for the 5′-maturation of 16 S rRNA is a 5′-end-dependent ribonuclease that has context-dependent broad sequence specificity. *J. Biol. Chem.* **275**, 8726–8732 (2000).
28. Song, W. et al. Antibiotic stress-induced modulation of the endoribonucleolytic activity of RNase III and RNase G confers resistance to aminoglycoside antibiotics in *Escherichia coli*. *Nucleic Acids Res.* **42**, 4669–4681 (2014).
29. Byrgazov, K., Vesper, O. & Moll, I. Ribosome heterogeneity: another level of complexity in bacterial translation regulation. *Curr. Opin. Microbiol.* **16**, 133–139 (2013).
30. Simsek, D. & Barna, M. An emerging role for the ribosome as a nexus for post-translational modifications. *Curr. Opin. Cell Biol.* **45**, 92–101 (2017).
31. Xue, S. & Barna, M. Specialized ribosomes: a new frontier in gene regulation and organismal biology. *Nat. Rev. Mol. Cell Biol.* **13**, 355–369 (2012).
32. Thomas, J. G. & Baneyx, F. Roles of the *Escherichia coli* small heat shock proteins IbpA and IbpB in thermal stress management: comparison with ClpA, ClpB, and HtpG in vivo. *J. Bacteriol.* **180**, 5165–5172 (1998).
33. Albery, W. J. & Knowles, J. R. Free-energy profile of the reaction catalyzed by triosephosphate isomerase. *Biochemistry* **15**, 5627–5631 (1976).
34. Knowles, J. R. Enzyme catalysis: not different, just better. *Nature* **350**, 121–124 (1991).
35. Elmahdi, S., DaSilva, L. V. & Parveen, S. Antibiotic resistance of *Vibrio parahaemolyticus* and *Vibrio vulnificus* in various countries: a review. *Food Microbiol.* **57**, 128–134 (2016).
36. Horseman, M. A. & Surani, S. A comprehensive review of *Vibrio vulnificus*: an important cause of severe sepsis and skin and soft-tissue infection. *Int. J. Infect. Dis.* **15**, e157–e166 (2011).
37. Lee, K., Varma, S., SantaLucia, J. Jr & Cunningham, P. R. In vivo determination of RNA structure–function relationships: analysis of the 790 loop in ribosomal RNA. *J. Mol. Biol.* **269**, 732–743 (1997).
38. Orelle, C. et al. Protein synthesis by ribosomes with tethered subunits. *Nature* **524**, 119–124 (2015).
39. Moll, I., Hirokawa, G., Kiel, M. C., Kaji, A. & Blasi, U. Translation initiation with 70S ribosomes: an alternative pathway for leaderless mRNAs. *Nucleic Acids Res.* **32**, 3354–3363 (2004).
40. Karamyshev, A. L., Karamysheva, Z. N., Yamami, T., Ito, K. & Nakamura, Y. Transient idling of posttermination ribosomes ready to reinitiate protein synthesis. *Biochimie* **86**, 933–938 (2004).
41. Blomfield, I. C., Vaughn, V., Rest, R. F. & Eisenstein, B. I. Allelic exchange in *Escherichia coli* using the *Bacillus subtilis sacB* gene and a temperature-sensitive pSC101 replicon. *Mol. Microbiol.* **5**, 1447–1457 (1991).
42. Higuchi, R. in *PCR Technology: Principles and Applications for DNA Amplification* (ed. Erlich, H.A.) Ch. 6 (Palgrave Macmillan, London, 1989).
43. Moazed, D., Stern, S. & Noller, H. F. Rapid chemical probing of conformation in 16 S ribosomal RNA and 30 S ribosomal subunits using primer extension. *J. Mol. Biol.* **187**, 399–416 (1986).
44. Powers, T. & Noller, H. F. A functional pseudoknot in 16S ribosomal RNA. *EMBO J.* **10**, 2203–2214 (1991).
45. Ingolia, N. T. Genome-wide translational profiling by ribosome footprinting. *Methods Enzymol.* **470**, 119–142 (2010).
46. Li, H. & Durbin, R. Fast and accurate short read alignment with Burrows–Wheeler transform. *Bioinformatics* **25**, 1754–1760 (2009).
47. Mortazavi, A., Williams, B. A., McCue, K., Schaeffer, L. & Wold, B. Mapping and quantifying mammalian transcriptomes by RNA-seq. *Nat. Methods* **5**, 621–628 (2008).
48. Tarazona, S., Garcia-Alcalde, F., Dopazo, J., Ferrer, A. & Conesa, A. Differential expression in RNA-seq: a matter of depth. *Genome Res.* **21**, 2213–2223 (2011).
49. Nagaraj, N. et al. System-wide perturbation analysis with nearly complete coverage of the yeast proteome by single-shot ultra HPLC runs on a bench top Orbitrap. *Mol. Cell. Proteomics* **11**, M111.013722 (2012).
50. Wisniewski, J. R., Zougman, A., Nagaraj, N. & Mann, M. Universal sample preparation method for proteome analysis. *Nat. Methods* **6**, 359–362 (2009).
51. Rappsilber, J., Mann, M. & Ishihama, Y. Protocol for micro-purification, enrichment, pre-fractionation and storage of peptides for proteomics using StageTips. *Nat. Protoc.* **2**, 1896–1906 (2007).
52. Wisniewski, J. R., Zougman, A. & Mann, M. Combination of FASP and StageTip-based fractionation allows in-depth analysis of the hippocampal membrane proteome. *J. Proteome Res.* **8**, 5674–5678 (2009).
53. Bekker-Jensen, D. B. et al. An optimized shotgun strategy for the rapid generation of comprehensive human proteomes. *Cell Syst.* **4**, 587–599 (2017).
54. Cox, J. & Mann, M. MaxQuant enables high peptide identification rates, individualized p.p.b.-range mass accuracies and proteome-wide protein quantification. *Nat. Biotechnol.* **26**, 1367–1372 (2008).
55. Bolstad, B. M., Irizarry, R. A., Astrand, M. & Speed, T. P. A comparison of normalization methods for high density oligonucleotide array data based on variance and bias. *Bioinformatics* **19**, 185–193 (2003).
56. Tyanova, S. et al. The Perseus computational platform for comprehensive analysis of (prote)omics data. *Nat. Methods* **13**, 731–740 (2016).
57. Bassler, B. L., Wright, M., Showalter, R. E. & Silverman, M. R. Intercellular signalling in *Vibrio harveyi*: sequence and function of genes regulating expression of luminescence. *Mol. Microbiol.* **9**, 773–786 (1993).
58. Amarasinghe, A. K., Calin-Jageman, I., Harmouch, A., Sun, W. & Nicholson, A. W. *Escherichia coli* ribonuclease III: affinity purification of hexahistidine-tagged enzyme and assays for substrate binding and cleavage. *Methods Enzymol.* **342**, 143–158 (2001).
59. Totemeyer, S., Booth, N. A., Nichols, W. W., Dunbar, B. & Booth, I. R. From famine to feast: the role of methylglyoxal production in *Escherichia coli*. *Mol. Microbiol.* **27**, 553–562 (1998).
60. Heo, J. et al. RraAS2 requires both scaffold domains of RNase ES for high-affinity binding and inhibitory action on the ribonucleolytic activity. *J. Microbiol.* **54**, 660–666 (2016).
61. Lenz, D. H. et al. The small RNA chaperone Hfq and multiple small RNAs control quorum sensing in *Vibrio harveyi* and *Vibrio cholerae*. *Cell* **118**, 69–82 (2004).

Acknowledgements

We thank K.-H. Lee, Y. Lee and S. N. Cohen for helpful comments. This research was supported by the National Research Foundation of Korea (NRF) funded by the Ministry of Science, ICT and Future Planning (grant no. 2018R1A5A1025077 and 2017R1A2B2011008 to K.L.; grant no. 2015R1A5A1008958 to J.B. and H.-K.C.; grant no. 2017R1D1A1B03032197 to W.S.; and grant no. 2018R1D1A1B07050434 to J.-H.Y.).

Author contributions

W.S., M.J., J.-H.Y., E.S., M.L., Y.-I.K. and R.S. performed the experiments. Y.H., H.-K.C., J.H., J.E.L., C.J.M., Y.-H.K., S.E., Y.H., J.B. and K.L. analysed and interpreted the data. W.S., M.J., J.-H.Y., E.S., M.L., J.B. and K.L. wrote and reviewed the manuscript. J.B. and K.L designed the study, developed the methodology and supervised the study. All authors discussed the results and commented on the manuscript.

Competing interests

The authors declare no competing interests.

Additional information

Supplementary information is available for this paper at https://doi.org/10.1038/s41564-018-0341-1.

Reprints and permissions information is available at www.nature.com/reprints.

Correspondence and requests for materials should be addressed to J.B. or K.L.

Publisher's note: Springer Nature remains neutral with regard to jurisdictional claims in published maps and institutional affiliations.

© The Author(s), under exclusive licence to Springer Nature Limited 2019